Available online at BCREC Website: https://bcrec.id

Bulletin of Chemical Reaction Engineering & Catalysis, 15 (3) 2020, 861-873

Research Article

Synthesis and Characterization of $Bi_{13}B_{0.48}V_{0.49-x}P_xO_{21.45}$ and Efficient Catalyst for the Synthesis of 2,3-dihydroquinazolin-4(1H)-ones Derivatives Synthesis

Hanane Barebita*, Youssef Merroun, Soumya Ferraa, Abderrazak Nimour, Abdelaziz Souizi, Taoufiq Guedira

Laboratory of Organic, Inorganic Chemistry, Electrochemistry and Environment, Faculty of Science, University of Ibn Tofail, B.P. 133, 14000 Kenitra, Morocco.

Received: 6th July 2020; Revised: 1st December 2020; Accepted: 2nd December 2020; Available online: 19th December 2020; Published regularly: December 2020

Abstract

A new compound has been found in the system $Bi_{13}B_{0.48}V_{0.49-x}P_xO_{21.45}$ (with $0 \leq x \leq 0.34$), were prepared by the direct solid-state reaction of Bi_2O_3, $(NH_4)_2HPO_4$, V_2O_5, and B_2O_3. This material melts congruently and it crystallize with the sillenite structure (space group I23) and form a solid solution with the cubic lattice parameter increasing from with a = 10.1568 Å to 10.1436 Å with increasing of P_2O_5 molar. Consequently, the new composites belong to γ-variety of solid state. The samples have been characterized by Fourier transform infrared spectroscopy (FT-IR), diffraction XRD and scanning electron microscopy (SEM) coupled to the EDX. On the other hand, the valorization of the prepared composites was performed by using them as heterogeneous catalyst in the 2,3-dihydroquinazolin-4(1H)-ones derivatives synthesis. The catalyst is stable (as a bench top catalyst) and reusable.

Keywords: $Bi_{13}B_{0.48}V_{0.49-x}P_xO_{21.45}$; Heterogeneous catalyst; 2,3-dihydroquinazolin-4(1H)-ones; γ-Bi_2O_3; Solid state

How to Cite: Barebita, H., Merroun, Y., Ferraa, S., Nimour, A., Souizi, A., Guedira, T. (2020). Synthesis and Characterization of $Bi_{13}B_{0.48}V_{0.49-x}P_xO_{21.45}$ and Efficient Catalyst for the Synthesis of 2,3-dihydroquinazolin-4(1H)-ones Derivatives Synthesis. *Bulletin of Chemical Reaction Engineering & Catalysis*, 15(3), 861-873 (doi:10.9767/bcrec.15.3.9224.861-873)

Permalink/DOI: https://doi.org/10.9767/bcrec.15.3.9224.861-873

1. Introduction

Metal oxides have been recognized as catalysts for various applications. Some notable examples of these solids used in heterogeneous environmental photocatalysis include TiO_2, ZnO, Bi_2O_3, CdS, WO_3, SnO_2, ZnS, CdTe, CdTe, Fe_2O_3, $AgNbO_3$, and $SrTiO_3$ [1]. Bi_2O_3 is an important inorganic functional material. It has been the subject of particular attention due to its unique electrical and optical properties, which has led to its widespread use in catalysis [2–4], optical coatings [5], microelectronics [6,7], solid fuel cells [8], gas sensors, and glass manufacturing. In addition, it is a promising photocatalyst in visible light with a narrow band gap 2.6–2.9 eV [9,10]. Moreover, catalysis by mixed oxides is an important area for the development of heterogeneous catalysts used in various applications.

Transition metal oxides and in particular mixed oxides have long attracted great technological and industrial interest. Due to their di-

* Corresponding Author.
Email: hanane.barebita@gmail.com (H. Barebita)

verse properties and to their thermal stability, these mixed oxides can be used as supports [11,12].

This is how we began the study of a continuous series of solid solution $Bi_{13}B_{0.48}V_{0.49-x}P_xO_{21.45}$ ($0 \leq x \leq 0.34$), which was prepared by solid treatment and crystallizes in a sillenite type structure. The synthesized products are structurally characterized by X-ray diffraction (XRD), Fourier Transform Infrared Spectroscopy (FTIR), scanning electron microscopy (SEM) and dispersive energy (EDX). In order to test the catalytic activity of these new supports in the synthesis of 2,3-dihydroquinazolin-4(1H)-one.

2. Materials and Methods

2.1 Materials and Instrumentation

The characterization of the prepared phases is carried out by X-ray diffraction on powder using a SIEMENS 5000 diffractometer from the PANALYTICAL company with copper anticathode (k Cu=1.5406 Å), the different diagrams obtained are recorded at room temperature, in a wide angular range ($20° \leq 2\theta \leq 60°$) with a step of 0.06° and for a counting time of 40 s. XRD data processing is performed by X'Pert Highscore Plus. The intermediate and final compounds resulting from the thermal decomposition of the precursors were analysed using Fourier Transform Infrared Spectrophotometer (FTIR) ALPHA.

The morphology and size of the synthesized powders were examined by scanning electron microscopy SUPRA 40 VP GEMINI ZEISS COLUMN, coupled with an EDX type analyzer (Energy Dispersive X-Rays Spectroscopy, Oxford instruments X-Max 20 mm^2) to determine the local quantitative elemental composition of a sample, with a maximum resolution of 1 µm at voltages ranging from 10 to 25 kV.

All chemicals used in this study were purchased from Aldrich and Fluka and are used without further purification. The synthesized products were characterized by their physical properties and by comparison with authentic samples that exist in the literature. The ^1H NMR spectra were recorded on an advanced 300 MHz Bruker instrument and the ^{13}C NMR data were collected on Bruker Advanced 75 MHz.

2.2 Preparation of $Bi_{13}B_{0.48}V_{0.49-x}P_xO_{21.45}$ Phase

Samples of general formula $Bi_{13}B_{0.48}V_{0.49-x}P_xO_{21.45}$ in the composition range $0 \leq x \leq 0.34$ were prepared by standard solid–state methods. Appropriate amounts of Bi_2O_3, B_2O_3, $((NH_4)_2HPO_4)$ and V_2O_5, were grounded together in an agate mortar. The dried powders were heated at 350 °C for 15 hours. After this first heating, the mixtures are removed from the oven, and finely ground and then heated a second time at a temperature of 700 °C for 15 hours. The simples were ground into powder for characterization.

2.3 General Procedure for the 2,3-dihydroquinazolin-4(1H)-ones Derivatives Synthesis

A mixture of (1 mmol) anthranilamide and (1 mmol) aromatic aldehyde in (3 mL) ethanol were reacted in the presence of $Bi_{13}B_{0.48}V_{0.49-x}P_xO_{21.45}$ with ($0 \leq x \leq 0.34$) (Scheme 1). The mixture was stirred under reflux for 10 to 40 min. The reaction is followed by (TLC) (Chloroform/Methanol, 8/2). After completion of the reaction, the mixture was cooled at room temperature. Then, dichloromethane (5 mL) was added to the mixture to separate the catalyst by simple filtration; the filtrate was evaporated until the precipitates were formed. The product was purified by recrystallization with ethanol to obtain the 2,3-dihydroquinazolin-4(1H)-ones. The catalyst may be reactivated later by washing with ethanol to remove the products that may be present on its surface and then dried before being reused. The products obtained 3a-3g are identified by the spectroscopic methods NMR H^1, NMR C^{13} as follow:

2-Phenyl-2,3-dihydroquinazolin-4(1H)-one 3a: ^1H NMR(300 MHz, DMSO-d_6, delta, ppm): 8.30 (1H, s, NHCO), 7.64 (1H, d, ^3J = 1.5 Hz, Ar-H), 7.51 (2H, d, ^3J = 1.5 Hz, Ar-H), 7.40 (3H, m), 7.25 (1H, t, ^3J = 8.8 Hz, Ar-H), 7.12 (1H, s, NH), 6.76 (1H, d, ^3J = 7.7 Hz, Ar-H), 6.69 (1H, t, ^3J = 7.11 Hz, Ar-H), 5.77 (1H, s, CH). ^{13}C NMR (75 MHz, DMSO-d_6): δ 164.08, 148.35, 142.10, 133.79, 128.93, 128.80, 127.83, 127.34, 117.59, 115.43, 114.88, 67.05.

2-(4-Methyphenyl)-2,3-dihydroquinazolin-4(1H)-one 3b: ^1H NMR (300 MHz, DMSO-d_6, delta, ppm): 8.23 (1H, s, NHCO), 7.61 (1H, d, ^3J = 7.8 Hz, Ar-H), 7.37 (2H, d, ^3J = 8.1 Hz, Ar-H), 7.27-7.18 (3H, m), 7.05 (1H, s, NH), 6.74 (1H, d, ^3J = 8.1 Hz, Ar-H), 6.67 (1H, t, ^3J = 8 Hz, Ar-H), 5.71 (1H, s, CH), 2.30 (3H, s, CH_3). ^{13}C NMR (75 MHz, DMSO-d_6): δ 164.10, 148.38, 139.13, 138.87, 133.18, 133.72, 129.27, 127.80, 127.26, 117.53, 115.47, 114.87.25, 66.84, 21.19.

2-(4-Chlorophenyl)-2,3-dihydroquinazolin-4(1H)-one 3c: ^{1}H NMR(300 MHz, DMSO-d$_6$, delta, ppm): 8.35 (1H, s, NHCO), 7.63 (1H, d, ^{3}J = 6.6 Hz, Ar-H), 7.54-7.45 (4H, m), 7.26 (1H, t, ^{3}J = 6.9 Hz, Ar-H), 7.15 (1H, s, NH), 6.76 (1H, d, ^{3}J = 7.8 Hz, Ar-H), 6.69 (1H, t, ^{3}J = 7.2 Hz, Ar-H), 5.79 (1H, s, CH). ^{13}C NMR (75 MHz, DMSO-d$_6$): δ 163.98, 148.13, 141.13, 133.87, 133.46, 129.23, 128.78, 127.85, 117.76, 115.42, 114.94, 66.25.

2-(4-Nitrophenyl)-2,3-dihydroquinazolin-4(1H)-one 3d: ^{1}H NMR ((300 MHz, DMSO-d$_6$, delta, ppm): 8.53 (1H, s, NHCO), 8.25 (2H, d, ^{3}J = 9 Hz, Ar-H), 7.75 (2H, d, ^{3}J = 8.7 Hz, Ar-H), 7.62 (1H, d, ^{3}J = 7.8 Hz, Ar-H), 7.34 (1H, s, NH), 7.27 (1H, t, ^{3}J = 7.8 Hz, Ar-H), 6.78 (1H, d, ^{3}J = 7.8 Hz, Ar-H), 6.69 (1H, t, ^{3}J = 7.2 Hz, Ar-H), 5.93 (1H, s, CH). ^{13}C NMR (75 MHz, DMSO-d$_6$): δ 163.76, 149.78, 147.89, 147.71, 134.04, 129.28, 128.05, 127.88, 124.57, 124.05, 117.94, 115.37, 115.02, 65.77.

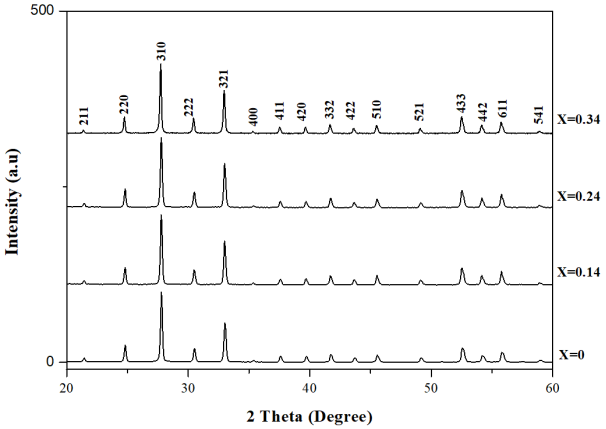

Figure 1. X-Ray Diffraction of $Bi_{13}B_{0.48}V_{0.49-x}P_xO_{21.45}$ with ($0 \leq x \leq 0.34$).

2-(4-Dimethylaminophenyl)-2,3-dihydroquinazolin-4(1H)-one (3e): ^{1}H NMR (300 MHz, DMSO-d$_6$), δ (ppm): 8.06 (1H, s, NHCO), 7.62 (1H, d, ^{3}J = 8.5 Hz, Ar-H), 7.24 (1H, t, ^{3}J = 8.7 Hz, Ar-H), 7.10-7.03 (5H, m, Ar-H), 6.82 (1H, s, NH), 6.74 (1H, d, ^{3}J = 8.1 Hz, Ar-H), 6.68 (1H, t, ^{3}J = 7.5 Hz, Ar-H), 6.03 (1H, s, CH), 2.89 (6H, s, N(CH$_3$)$_2$). ^{13}C NMR (75 MHz, DMSO-d$_6$), δ (ppm): 163.82, 162.45, 152.36, 148.230, 133.17, 128.94, 128.72, 127.76, 116.98, 115.14, 114.53, 111.13, 66.68, 40.15.

2-(4-Methoxyphenyl)-2,3-dihydroquinazolin-4(1H)-one 3f: ^{1}H NMR(300 MHz, DMSO-d$_6$, delta, ppm): 8.21 (1H, s, NHCO), 7.63 (1H, d, ^{3}J = 7.5 Hz, Ar-H), 7.43 (2H, d, ^{3}J = 7.8 Hz, Ar-H), 7.22 (1H, t, ^{3}J = 7.8 Hz, Ar-H), 7.03 (1H, s, NH), 6.94 (2H, d, ^{3}J = 8.7 Hz, Ar-H), 6.76 (1H, d, ^{3}J = 8.1 Hz, Ar-H), 6.67 (1H, t, ^{3}J = 7.5 Hz, Ar-H), 5.73 (1H, s, CH), 3.75 (3H, s, OCH$_3$). ^{13}C NMR (75 MHz, DMSO-d$_6$): δ 164.23, 159.92, 148.51, 133.91, 133.71, 128.71, 127.84, 117.58, 115.48, 114.90, 114.10, 66.84, 55.63.

Table 1. Evolution of angular positions and intensities of $Bi_{13}B_{0.48}V_{0.49-x}P_xO_{21.45}$ phases.

hkl	x=0			x=0.14			x=0.24			x=0.34		
	d_{obs} (Å)	d_{cal} (Å)	I/I_0	d_{obs} (Å)	d_{cal} (Å)	I/I_0	d_{obs} (Å)	d_{cal} (Å)	I/I_0	d_{obs} (Å)	d_{cal} (Å)	I/I_0
2 0 0	5.0844	5.0835	2	5.0831	5.0760	2.80	5.083	5.0839	1.85	5.072	5.0737	3.97
2 1 1	4.1440	4.1443	5	4.1503	4.1439	5.05	4.1464	4.1451	4.80	4.1428	4.1435	4.99
2 2 0	3.5904	3.5898	23	3.593	3.5892	25.53	3.5894	3.5892	23.19	3.5872	3.5876	24.26
3 1 0	3.2110	3.2108	100	3.214	3.2101	100.00	3.209	3.2100	100.00	3.208	3.2088	100.00
2 2 2	2.9318	2.9314	22	2.9342	2.9305	22.78	2.9304	2.9304	21.03	2.9287	2.9289	21.16
3 2 1	2.7130	2.7138	67	2.7172	2.7132	63.86	2.7135	2.7133	62.86	2.7116	2.7116	59.57
4 0 0	2.5401	2.5390	4	2.536	2.5369	2.32	2.5391	2.5389	3.42	2.5376	2.5361	2.19
4 11	2.3920	2.3937	10	2.3963	2.3926	10.27	2.3922	2.3926	8.01	2.3915	2.3911	8.70
4 2 0	2.2714	2.2709	10	2.2740	2.2696	10.11	2.27	2.2699	9.86	2.2682	2.2681	9.02
3 3 2	2.1661	2.1651	15	2.1678	2.1644	14.58	2.164	2.1642	13.35	2.1630	2.1626	13.25
4 2 2	2.0711	2.0728	9	2.0763	2.0727	8.03	2.0726	2.0723	8.46	2.071	2.0704	7.15
5 1 0	1.9899	1.9914	13	1.9945	1.9908	12.87	1.991	1.9909	15.44	1.9901	1.9896	11.17
5 2 1	1.8533	1.8541	9	1.8568	1.8532	6.98	1.8541	1.8537	9.54	1.8530	1.8520	6.77
4 3 3	1.7430	1.7413	29	1.7445	1.7411	30.64	1.7415	1.7410	29.86	1.7404	1.7395	24.32
4 4 2	1.6931	1.6923	14	1.6955	1.6923	14.24	1.6929	1.6924	15.25	1.6913	1.6904	10.69
6 1 1	1.6479	1.6471	19	1.6491	1.6470	24.09	1.6477	1.6469	21.09	1.6463	1.6455	17.07
5 4 1	1.5654	1.5664	3	1.5686	1.5670	3.63	1.5674	1.5665	3.80	1.5660	1.5660	2.80

2 - (2 , 3 - D i m e t h o x y p h e n y l) - 2 , 3 - dihydroquinazolin-4(1H)-one 3g: ^{1}H NMR(300 MHz, DMSO-d_6, delta, ppm): 8.05 (1H, s, NHCO), 7.65 (1H, d, ^{3}J = 8.5 Hz, Ar-H), 7.27-7.22 (1H, t, ^{3}J = 8.7 Hz, Ar-H), 7.11-7.03 (3H, m), 6.81 (1H, s, NH),6.78-6.67 (2H, m), 6.06 (1H, s, CH), 3.83 (3H, s, OCH_3), 3.81 (3H, s, OCH_3). ^{13}C NMR (75 MHz, DMSO-d_6): δ 164.24, 152.72, 148.47, 146.60, 134.94, 133.72, 127.80, 124.37, 119.56, 117.54, 115.20, 114.91, 113.47, 61.69, 61.19, 56.28.

3. Results and Discussions

3.1 Characterization of Catalysts

The X-ray crystallographic analysis was performed for the phases obtained within the quaternary system Bi_2O_3-B_2O_3-P_2O_5-V_2O_5, the substitution of vanadium by phosphorus revealed the existence of a total solid solution of the selenite type of formula $Bi_{13}B_{0.48}V_{0.49-x}P_xO_{21.45}$ with ($0 \leq x \leq 0.34$). The four samples were analyzed by X-ray diffraction and the results obtained are presented in Figure 1.

These samples are identified by comparing the experimental diagrams with the reference data of the JCPDS standard data (Joint Committee for Powder Diffraction Standards). All the observed diffraction peaks can be indexed to the standard data of $Bi_{13}B_{0.48}V_{0.49-x}P_xO_{21.45}$ with card No 00-044-0425. The progressive substitution of vanadium by phosphorus shows the existence of a pure phase which crystallizes in a cubic system of space group I23 with a = 10.1568 Å for x = 0, a = 10.1536 Å for x = 0.14, a = 10.1518 Å for x = 0.24 and a = 10.1436 Å for x = 0.34. This phase will be designated throughout this work by γ-Bi_2O_3.

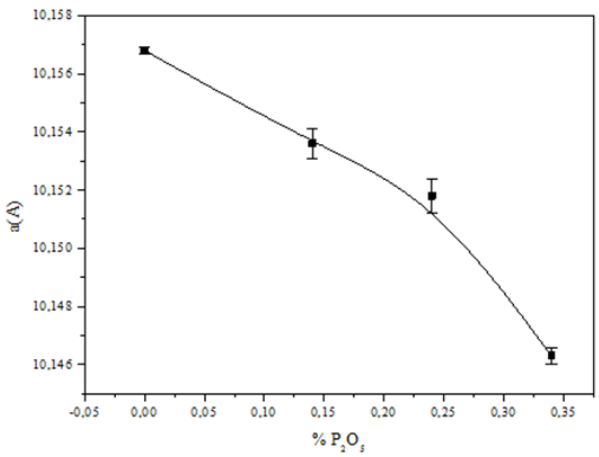

Figure 2. Variation of cubic cell parameter a as a function of P_2O_5.

The various compositions of the solid solution are perfectly indexed in the cubic system. Table 1 shows the indexing of the diffraction peaks and the observed and calculated reticular distances. The cell parameter was refined by TREOR 90, a sub-program of the Full prof software. After searching for peaks in each spectrum and eliminating Kα2 peaks, the data is saved in a TREOR format to generate a data file. The refinement results are displayed in output files. The variations in the "a" cell parameter are shown in Figure 2.

From Figure 2, it can be seen that the linear decrease in the mesh parameter is due to the difference in the size of the ionic rays of the phosphorus and vanadium cations of the same coordination (V). In effect, by replacing the P^{5+} ions of ionic ray with V^{5+} ions, a small cation is replaced by a large cation, which favours the observed decrease. This shows that the substitution of phosphorus by vanadium leads to the formation of a solid solution (sillenite type).

Another information that we can extract from X-ray diffraction diagrams is the average crystalline crystal size. Indeed, Scherrer [13,14] has shown that the size of the particles is inversely proportional to the width of the diffraction peaks. This crystal size can be obtained by applying the following relation (Equation 1).

$$D = \frac{K \times \lambda}{(\cos\theta) \times \beta} \quad (1)$$

Table 2 shows the average sizes *D* of the various samples produced.

Table 2. Average crystallite size of $Bi_{13}B_{0.48}V_{0.49-x}P_xO_{21.45}$ phase.

Fraction x	x=0	x=0.14	x=0.24	x=0.34
2θ (°)	27.7623	27.7687	27.7684	27.7800
θ (°)	13.88115	13.88435	13.8842	13.89
cos θ	0.970795	0.970782	0.970782	0.970758
$h_{1/2}$(radian)	0.0024731	0.0025656	0.0026005	0.0027401
Cosθ× $h_{1/2}$	0.00240087	0.0024906	0.00252452	0.00265997
D (nm)	57.753248	55.670922	54.922916	52.126151

It can be seen that the average size of the crystallites *D* of the cubic phase decreases as a function of x. This leads to the conclusion that the average size of the crystallites depends on the composition of the solid solution and that the substitution of phosphorus by vanadium leads to the formation of smaller crystallites, which is a priori of interest for catalysis. The reduction in grain size leads to an increase in the specific area, which results in an increase in catalytic activity [15].

The infrared spectra of $Bi_{13}B_{0.48}V_{0.49-x}P_xO_{21.45}$ with ($0 \leq x \leq 0.34$) are recorded at room temperature in the frequency range between 100 and 400 cm^{-1} as shown in Figure 3. The observed bands along with their vibrational assignments of samples have been tabulated in Table 3.

The IR spectra show a band around 1387 cm^{-1} which is attributed to the asymmetric stretching mode B–O in the orthoborate units (BO_3) [31]. It can be attributed to the vibrations of the B–O– bonds as well as to the vibrations of B–O bonds present in borate rings [32]. The band at 1072 cm^{-1}, corresponding to ($vasPO_3$) moves towards the high frequencies at 1094 cm^{-1} this is due to the changes in angular connection inside the chains P–O–P [29,30]. Indeed a new band emerges in the infrared spectra at 960 cm^{-1}. This band is due to the simultaneous vibration isolated V=O groups in a vanadyl bipyramid triangular base VO_5 and the symmetric vibration PO_3 ($vsPO_3$) [26–28]. The band around about 845 cm^{-1} correspond more particularly to vibration elongations of the Bi-O bonds in the pyramid units [BiO_3] [25]. However the band near 760 cm^{-1} has been assigned to asymmetric stretching modes (vas POP) [20–24]. The band around 660 cm^{-1} contributing to the vibrations of BO_4 units and would correspond more particularly to the vibrations of BO_4 units present in rings such as diborate units, or tri, tetra or pentaborate units [19]. The band at 570 cm^{-1} is attributed to the vibrations of the V–O–V links in VO_4 tetrahedra [18]. Finally, the band centred at 521 cm^{-1} may be attributed to the Bi–O–Bi stretching vibrations of BiO_6 Octahedral units [17] and another band situated at 430 cm^{-1} is assigned to the Bi–O vibration mode in the [BiO_6] configuration [16].

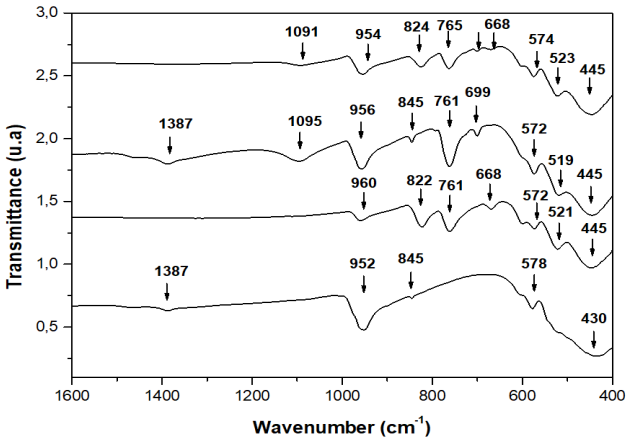

Figure 3. FT–IR spectra of $Bi_{13}B_{0.48}V_{0.49-x}P_xO_{21.45}$ phase.

Scanning electron microscopy provides information not only on the morphology, distribution and size of grains or agglomerates but also on the local chemical composition when coupled with an X-EDX analyzer shown in Figure 4.

Table 3. FT−IR data of the $Bi_{13}B_{0.48}V_{0.49-x}P_xO_{21.45}$ for the composition ($0 \leq x \leq 0.34$).

Band assignments	x=0	x=0.14	x=0.24	x=0.34	References
Bi–O vibrations of [BiO_6] octahedral units	430	445	445	445	[16]
Vibrations of Bi–O–Bi bonds strongly distorted BiO_6 units	------	521	519	523	[17]
Stretching vibration of V–O–V	578	572	572	574	[18]
Stretching vibration of tetra-borate groups of bridging in BO_4 units.	------	668	669	668	[19]
Asymmetric stretching vibrations of P–O–P (vas POP)	------	761	761	765	[20–24]
Stretching vibrations of Bi–O bond in BiO_3 pyramidal units	845	822	845	824	[25]
Vibration of V=O bonds isolated in bipyramids with triangular base and symmetric stretching vibrations bending modes of (v_sPO_3)	952	960	956	954	[26–28]
Asymmetric stretching vibrations ($v_{as}PO_3$)	------	------	1095	1091	[29,30]
Asymmetric stretching of B–O bond in BO_3 units	1387	------	1387	------	[31]

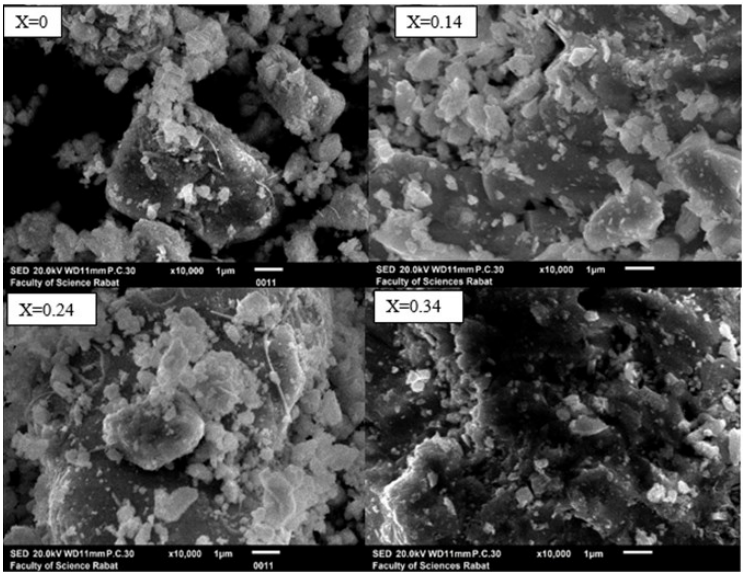

Figure 4. SEM images of the different catalysts synthesized composition $Bi_{13}B_{0.48}V_{0.49-x}P_xO_{21.45}$ with ($0 \leq x \leq 0.34$).

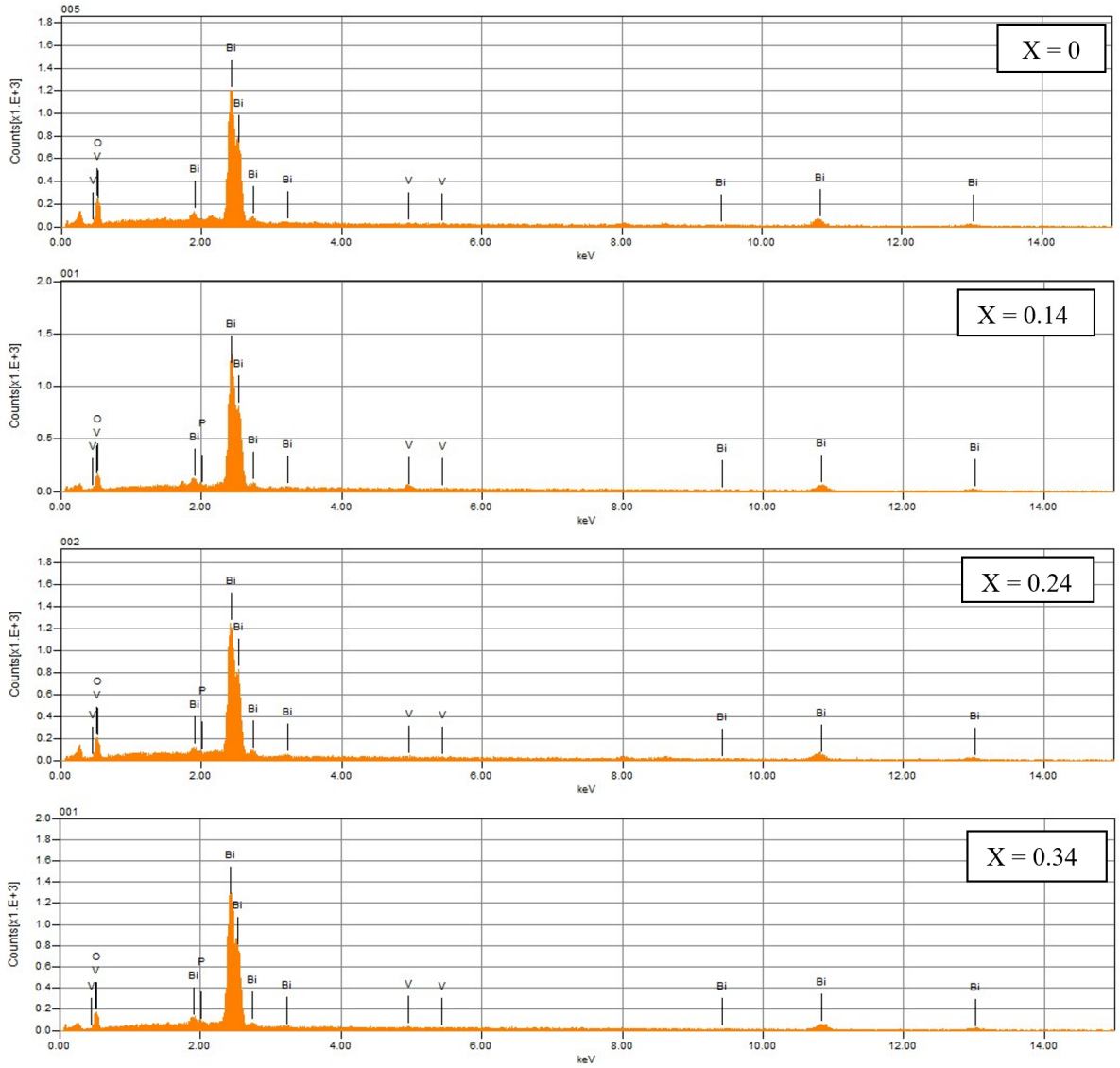

Figure 5. EDX spectra composition $Bi_{13}B_{0.48}V_{0.49-x}P_xO_{21.45}$ with ($0 \leq x \leq 0.34$).

The resulting images are shown in Figure 4, respectively. These images show a micrograph of particles that are globally heterogeneous and crystallized as randomly distributed clusters. The grains appear with different shapes and texture relative to the presence of some small holes, inside the compounds which are due to low porosity.

Table 4. Catalytic test for the 2,3-dihydroquinazolin-4(1H)-one synthesis.

Entry	$Bi_{13}B_{0.48}V_{0.49-x}P_xO_{21.45}$	Time (min)	Yield (%)
1	_	60	trace
2	x=0	10	87
3	x=0.14	18	83
4	x=0.24	20	80
5	x=0.34	25	78

To identify the elements contained in the synthesized powders and to determine their compositions an EDX chemical analysis was carried out on some prepared compositions (Figure 5). The spectra clearly show the presence of the chemical elements that make up the synthesized compounds without any element foreign to the materials.

3.2 Catalytic Test of $Bi_{13}B_{0.48}V_{0.49-x}P_xO_{21.45}$

The condensation between benzaldehyde and anthranilamide is chosen as a model reaction to test the catalytic activity of $Bi_{13}B_{0.48}V_{0.49-x}P_xO_{21.45}$ with ($0 \leq x \leq 0.34$). Firstly, the model reaction was carried out in the absence and presence of the catalyst. The results obtained are shown in the Table 4.

The results presented in Table 5 show that in the absence of catalyst, only traces of the product 3a obtained even after 60 min. While

Table 5. Solvent effect on the 2,3-dihydroquinazolin-4(1H)-one synthesis[a]

$Bi_{13}B_{0.48}V_{0.49-x}P_xO_{21.45}$	Solvent	Time (min)	Yield (%)[b]
x=0	EtOH	10	87
	MeOH	16	84
	Dioxane	27	75
	Acetonitrile	20	78
	Chloroforme	30	73
x=0.14	EtOH	18	83
	MeOH	23	80
	Dioxane	30	77
	Acetonitrile	24	79
	Chloroforme	37	76
x=0.24	EtOH	20	80
	MeOH	25	81
	Dioxane	38	73
	Acetonitrile	30	76
	Chloroforme	38	70
x=0.34	EtOH	25	78
	MeOH	28	77
	Dioxane	36	71
	Acetonitrile	32	73
	Chloroforme	40	67

[a]Reaction conditions: benzaldehyde (1 mmol), anthranilamide (1 mmol), catalyst amount (10 mg). [b]Isolated yields.

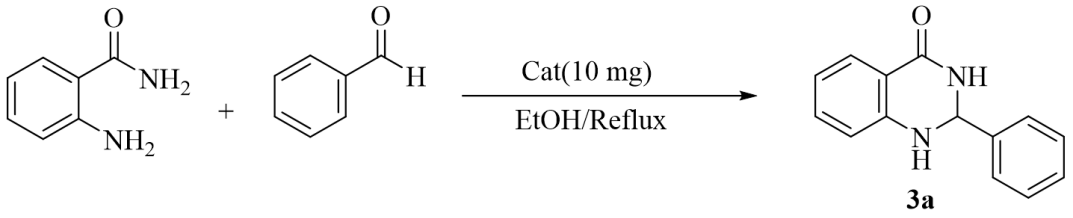

Scheme 1. The model reaction of 2,3-dihydroquinazolin-4(1H)-one synthesis.

in the presence of the catalysts $Bi_{13}B_{0.48}V_{0.49-x}P_xO_{21.45}$ with ($0 \leq x \leq 0.34$), the product 3a is obtained in short reaction times (10-25 min) with good yields (78-87%). These results clearly shows the interesting catalytic activity of the four catalysts used in the 2,3-dihydroquinazolin-4 (1H) -ones synthesis.

In addition, the comparison of the results obtained with x = 0 and that obtained with x = 0.14, x = 0.24 and x = 0.34, shows that a significant correlation exists between the catalysts and the catalytic activity, That is to say, when we go from x = 0 to 0.34, the catalytic activity decreases, which is explained by the decrease in the specific surface.

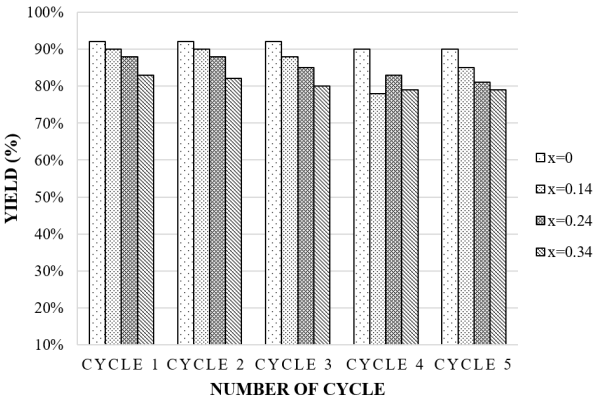

Figure 6. Reusability of the $Bi_{13}B_{0.48}V_{0.49-x}P_xO_{21.45}$ with ($0 \leq x \leq 0.34$) catalysts in the model reaction.

In order to optimize the reaction solvent, we examined the influence of the solvent on the yield of product 3a, by varying the nature of the reaction solvent, such as protic polar (Ethanol, Methanol), polar aprotic (Acetonitrile) and apolar aprotic (Chloroform, Dioxane). The yields obtained are summarize in Table 5. The results given in Table 5 show that the reaction is clearly favored in protic polar solvents and more specifically in ethanol, this is available for the model reaction where the $Bi_{13}B_{0.48}V_{0.49-x}P_xO_{21.45}$ with ($0 \leq x \leq 0.34$) catalysts were applied, the product 3a is obtained with yields which are 87, 83, 80, and 78% respectively. However, in the case of methanol it is noted that it allows obtaining the product with a lower yield than ethanol even though its dielectric constant is greater compared to the ethanol one, which may be explained by the fact that the methanol is more acidic than the ethanol, thus the O–H bond is more polar in methanol than in ethanol. Therefore, the methanol tends to liberate the proton more easily, unlike to the ethanol which just allows the polarization of the reagents leading to the formation of the desired product 3a with a good yield. Moreover, the appropriate solvent for each organic synthesis depends on the nature

Table 6. Influence of the catalyst amount on the 2,3-dihydroquinazolin-4(1H)-one synthesis[a]

$Bi_{13}B_{0.48}V_{0.49-x}P_xO_{21.45}$	Catalyst amount (mg)	Time (min)	Yield (%)[b]
x=0	3	10	89
	5	10	91
	7	10	92
	9	10	90
	10	10	87
x= 0.14	3	18	87
	5	18	88
	7	18	90
	9	18	87
	10	18	83
x= 0.24	3	20	86
	5	20	88
	7	20	85
	9	20	82
	10	20	80
x= 0.34	3	25	79
	5	25	81
	7	25	83
	9	25	79
	10	25	78

[a] Reaction conditions: benzaldehyde (1 mmol), anthranilamide (1 mmol), EtOH, catalyst amount (x mg). [b] Isolated yields

of the reaction mixture. Therefore, the use of ethanol as a solvent facilitates the formation and the separation of the charges on the active sites of the reagents, indeed this process is caused by the electrostatic interaction involved between the atomic charge on the atom forming polar bond of the solvent with the active atomic center which possesses the opposite sign of charge, in the reagent, this interaction makes easy the formation of the final product 3a.

As regards the aprotic polar solvents and apolar (Acetonitrile, Dioxane, Chloroform), used in this part of our study, one can notice that the yield obtained in presence of each solvent is lower than that obtained in ethanol. One can deduce that ethanol is the appropriate solvent allowing to obtain the desired product with excellent yields.

The next study of this work has been focused on the determination of the appropriate

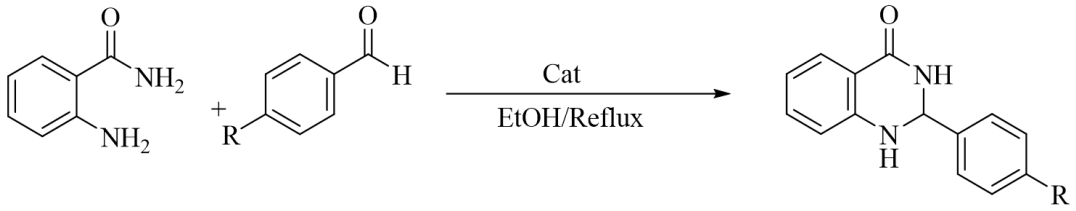

Scheme 2. 2,3-dihydroquinazolin-4(1H)-ones derivatives synthesis.

Table 7. Yields, reaction times and melting points for 2,3-dihydroquinazolin-4(1H)-one derivatives synthesis

Entry	R	$Bi_{13}B_{0.48}V_{0.49-x}P_xO_{21.45}$	Time (min)	Yield (%)	M.P (°C)	
					Found	Reported
3**a**	H	x= 0	10	92	219-220	218-220 [33]
		x= 0.14	18	90		
		x= 0.24	20	88		
		x= 0.34	25	83		
3**b**	4-CH_3	x= 0	22	92	232–233	233–234 [33]
		x= 0.14	26	89		
		x= 0.24	35	86		
		x= 0.34	30	82		
3**c**	4-Cl	x= 0	10	95	204-205	205–206 [34]
		x= 0.14	15	93		
		x= 0.24	20	90		
		x= 0.34	20	87		
3**d**	4-NO_2	x= 0	17	90	199-200	198–200 [34]
		x= 0.14	20	91		
		x= 0.24	32	91		
		x= 0.34	30	85		
3**e**	4-$N(CH_3)_2$	x= 0	23	90	227-228	227-228 [35]
		x= 0.14	33	88		
		x= 0.24	40	85		
		x= 0.34	40	80		
3**f**	4-OCH_3	x= 0	25	89	192-193	192–193 [36]
		x= 0.14	27	93		
		x= 0.24	34	86		
		x= 0.34	40	84		
3**g**	2,3-OCH_3	x= 0	28	87	220-221	220-221 [37]
		x= 0.14	30	88		
		x= 0.24	38	83		
		x= 0.34	40	80		

catalyst amount for the synthesis of product 3a. The model reaction has been realized in various catalyst amount from 3 to 10 mg. The results obtained are collated in Table 6.

From the results obtained (Table 6), we can clearly see the influence of the amount of catalyst on the yield. The best yield 92, 90, 83 and 88% has been obtained in presence optimum masses of the catalysts are 7 mg of x= 0, 0.14, 0.34 and 5 mg of x= 0.24 respectively.

The long-term durability of the catalyst must be also studied to prove its catalytic efficiency. For that, the model reaction was performed under the optimal conditions of solvent and catalyst amount. After reaction completion, the catalyst was recovered and washed

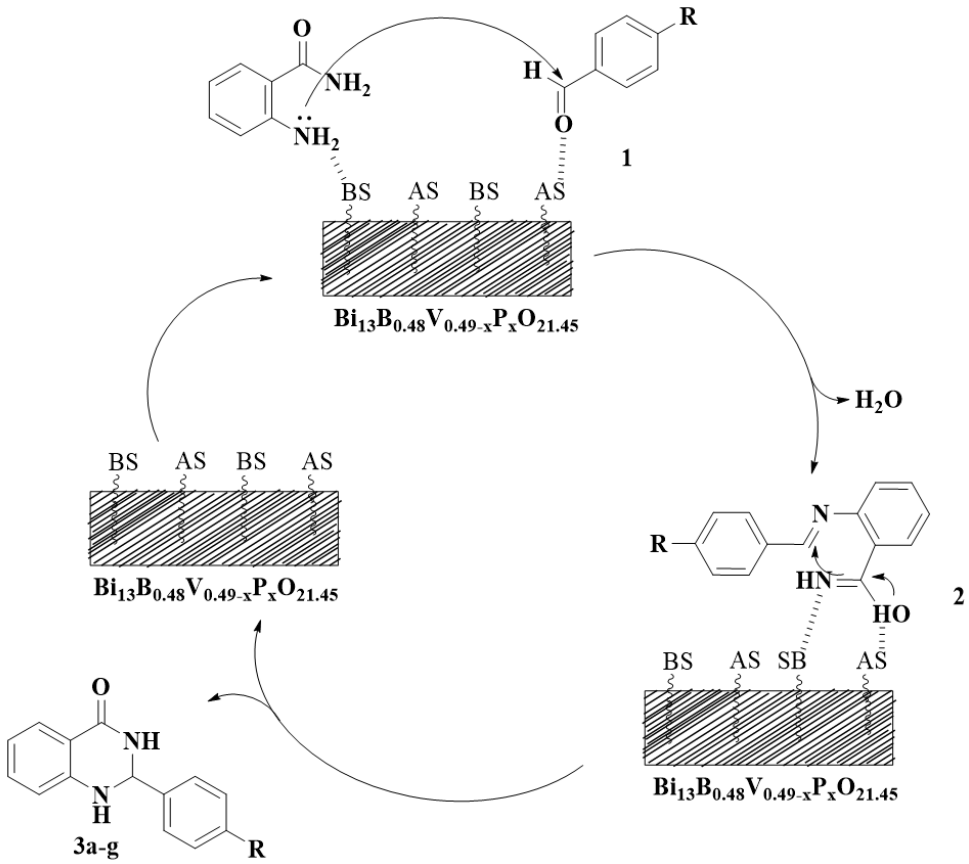

Scheme 3. A plausible mechanism for the formation of 2,3-dihydroquinazolin-4(3H)-ones.

Table 8. Comparison of $Bi_{13}B_{0.48}V_{0.49-x}P_xO_{21.45}$ ($0 \leq x \leq 0.34$) catalytic activity with different catalysts reported in the literature in the 2,3-dihydroquinazolin-4(1H)-one derivatives synthesis.

Catalysts	Reaction conditions	Time (min)	Yield (%)	Ref
X=0	EtOH, reflux	10	92	This work
X=0.14	EtOH, reflux	18	90	This work
X=0.24	EtOH, reflux	20	88	This work
X=0.34	EtOH, reflux	25	83	This work
Acide oxalique	H_2O:EtOH, 80 °C	48	86	[38]
$[MIMC_4SO_3H]$-$[HSO_4]$	Sans solvant, 110 °C	90	69	[39]
PEG-400	Sans solvant, 100–110 °C	10 h	85	[40]
$Fe_3O_4@SiO_2SO_3H$	EtOH, reflux	4 h	67	[41]
PSSA	EtOH, reflux	60	91	[42]
$Ce(L\text{-}Pro)_2]_2(Oxa)$	EtOH, 50–55 °C	4.5h	89	[43]

with EtOH, stirred for 10 min, then dried at 100 °C to be ready the next reuse. The obtained yields are presented in Figure 6. The results shown that the catalytic activity was not affected even after five cycles of reuse since the yield of product 3a remains almost unchanged.

For the generalization study of 2,3-dihydroquinazolin-4(1H)-one derivatives synthesis, the reaction was carried out under optimal conditions using various aromatic aldehydes with different functional groups to react with anthranilamide (Scheme 2). The obtained results are collected in Table 7. The results show that whatever the substituent (R) of the used aromatic aldehyde, the final product is obtained with an excellent (80–95%) yield in short reaction time (10–40 min). Indeed, the nature (donor/attractor) of the aldehyde substitution group has not a significant effect on the catalyst efficiency.

One of the key points to understand the reaction mechanism in heterogeneous catalysis is the determination of the active surface sites and the activation processes. The presence of a large population of electron pairs on the surface compounds, such as: B^{3+}, Bi^{3+}, V^{5+}, P^{5+}, and O^{2-} indicates that the surface of $Bi_{13}B_{0.48}V_{0.49-x}P_xO_{21.45}$ presents certainly multicatalytic active sites such as basic sites (BS) and acidic sites (AS).

The synthesis mechanism of 2,3-dihydroquinazolin-4(3H)-ones formation was mostly based on direct cyclocondensation process; the plausible mechanism for this reaction was proposed in Scheme 3. Initially, the acidic sites coordinate with the oxygen atom of the aldehyde and facilitate the nucleophilic attack the amino group of anthranilamide to form intermediate 2. Then, the product 2 is activated by catalyst to facilitate the intermolecular nucleophilic attack of nitrogen on the imine carbon to directly give the desired 2,3-dihydroquinazolin-4(3H)-ones (3a-g).

In order to estimate the efficiency of the used catalysts in the 2,3-dihydroquinazolin-4(1H)-one synthesis, a comparative study has been carried out between $Bi_{13}B_{0.48}V_{0.49-x}P_xO_{21.45}$ and other catalyst reported in the literature (Table 8). The results (Table 8) shows that the four catalysts possess interesting catalytic activity compared to other catalysts reported in the literature in terms of the obtained reaction time and yield concerning the 2,3-dihydroquinazolin-4(1H)-one synthesis.

4. Conclusions

The elaboration of $Bi_{13}B_{0.48}V_{0.49-x}P_xO_{21.45}$ with ($0 \le x \le 0.34$), gives a solid solution it behaves as good solid catalysts with a percentage reaching 92%. Catalytic activity decreases with increasing phosphorus. It can be seen that the average size of the crystallites D of the cubic phase (rich in bismuth) decreases as a function of x. This makes it possible to conclude that the average size of the crystallites depends on the composition of the solid solution and that the substitution of vanadium by phosphorus leads to the formation of smaller crystallites, which is a priori advantageous for catalysis. The ability to recycle and reuse these catalysts remains an important advantage which will allow the opening of a field to very broad applications.

References

[1] Gaya, U.I. (2013). Heterogeneous Photocatalysis Using Inorganic Semiconductor Solids. Springer Science & Business Media.

[2] Pan, C., Li, X., Wang, F., Wang, L. (2008). Synthesis of bismuth oxide nanoparticles by the polyacrylamide gel route. *Ceram. Int.*, 34, 439−441.

[3] Xiaohong, W., Wei, Q., Weidong, H. (2007). Thin bismuth oxide films prepared through the sol–gel method as photocatalyst. *J. Mol. Catal. A: Chem.*, 261, 167−171.

[4] Huang, Q., Wang, Q., Tao, T., Zhao, Y., Wang, P., Ding, Z., Chen, M. (2019). Controlled Synthesis of Bi_2O_3/TiO_2 Catalysts with Mixed Alcohols for the Photocatalytic Oxidation of HCHO. *Environ. Technol.,* 40, 1937–1947.

[5] Al Wazny, M.S., Salim, E.T., Bader, B.A., Fakhry, M.A. (2018). Synthesis of Bi_2O_3 Films, Studying Their Optical, Structural, and Surface Roughness Properties. *IOP Conf. Ser. Mater. Sci. Eng.,* 454, 012160.

[6] Zhu, G., Yang, W., Lv, W., He, J., Wen, K., Huo, W., Hu, J., Waqas, M., Dickerson, J.H., He, W. (2017). Facile Electrophoretic Deposition of Functionalized Bi_2O_3 Nanoparticles. *Mater. Des.,* 116, 359–364.

[7] Bandoli, G., Barreca, D., Brescacin, E., Rizzi, G.A., Tondello, E. (1996). Pure and Mixed Phase Bi_2O_3 Thin Films Obtained by Metal Organic Chemical Vapor Deposition. *Chem. Vap. Depos.,* 2, 238–242.

[8] Polat, Y., Arı, M., Dağdemir, Y. (2017). Thermal, Electrical and Structural Properties of $(Bi_2O_3)_{1-x-y}(Sm_2O_3)_x(CeO_2)_y$ Electrolytes for Solid Oxide Fuel Cells. *Phase Transit.,* 90, 387–398.

[9] Shi, Y., Luo, L., Zhang, Y., Chen, Y., Wang, S., Li, L., Long, Y., Jiang, F. (2017). Synthesis and characterization of α/ß-Bi_2O_3 with enhanced photocatalytic activity for 17α-ethynylestradiol. *Ceram. Int.,* 43, 7627−7635.

[10] Chen, R., Shen, Z.R., Wang, H., Zhou, H.J., Liu, Y.P., Ding, D.T., Chen, T.H. (2011). Fabrication of mesh-like bismuth oxide single crystalline nanoflakes and their visible light photocatalytic activity. *J. Alloys Compd.,* 509, 2588–2596.

[11] Wang, F., Jiang, J., Wang, B. (2019). Recent In Situ/Operando Spectroscopy Studies of Heterogeneous Catalysis with Reducible Metal Oxides as Supports. *Cat.,* 9, 477.

[12] Arfaoui, J., Ghorbel, A., Petitto, C., Delahay, G. (2017). Novel Vanadium Supported onto Mixed Molybdenum-Titanium Pillared Clay Catalysts for the Low Temperature SCR-NO by NH_3. *Chem. Eng. J.,* 356, 598−608.

[13] Bokuniaeva, A.O., Vorokh, A.S. (2019). Estimation of Particle Size Using the Debye Equation and the Scherrer Formula for Polyphasic TiO_2 Powder. *J. Phys. Conf. Ser.,* 1410, 012057.

[14] Pandya, S.G., Corbett, J.P., Jadwisienczak, W.M., Kordesch, M.E. (2016). Structural Characterization and X-Ray Analysis by Williamson–Hall Method for Erbium Doped Aluminum Nitride Nanoparticles, Synthesized Using Inert Gas Condensation Technique, Physica E Low Dimens. *Syst. Nanostruct.,* 79, 98–102.

[15] Bourja, L., Bakiz, B., Benlhachemi, A., Ezahri, M., Villain, S., Gavarri, J.R. (2010). Synthesis and characterization of nanosized $Ce_{1-x}bi_xo_{2-\delta}$ solid solutions for catalytic applications. *Journal of Taibah University for Science*, 4, 1–8.

[16] Ai, Z., Huang, Y., Lee, S., Zhang, L. (2011). Monoclinic α-Bi_2O_3 Photocatalyst for Efficient Removal of Gaseous NO and HCHO under Visible Light Irradiation. *J. of Alloys and Compd.,* 509, 2044–2049.

[17] Rajyasree, C., Rao, D.K. (2011). Spectroscopic investigations on alkali earth bismuth borate glasses doped with CuO. *J. Non-Cryst. Solids*, 357, 836–841.

[18] Hayakawa, S., Yoko, T., Sakka, S. (1995). IR and NMR structural studies on lead vanadate glasses. *J. Non-Cryst. Solids,* 183, 73–84.

[19] Doweidar, H., Saddeek, Y.B. (2009). FTIR and ultrasonic investigations on modified bismuth borate glasses. *J. Non-Cryst. Solid*, 355, 348–354.

[20] Jermoumi, T., Hafid, M., Toreis, N. (2002). Thermaland FTIR analysis of $(50-x)BaO_{-x}Fe_2O_{3-50}P_2O_5$ glasses. *Phys. Chem. Glasses,* 43, 129−132.

[21] Subbalakshimi, P., Sastry, P.S., Veeraiah, N. (2001). Dielectric relaxation and ac conduction phenomena in PbO-WO_3-P_2O_5 glass system. *Phys. Chem. Glasses,* 42: 307-314.

[22] Khawaja, E.E., Durrani, S.M.A., Al-Adel, F.F., Salim, M.A., Hussain, M.S. (1995). X-ray photoelectron spectroscopy and Fourier transform-infrared studies of transition metal phosphate. *J. Mater. Sci.,* 30, 225–234.

[23] Shih, P.Y., Chin, T.S. (1999). Effect of redox state of copper on the properties of P_2O_5-Na_2O-CuO glasses. *Mater. Chem. Phys.,* 60, 50–57.

[24] Dayanand, C., Bhikshamaiah, G., Tyagaraju, V.J., Salagram, M., Krishna Murthy, A.S.R. (1996). Structural investigations of phosphate glasses: a detailed infrared study of the $x(PbO)_{-(1-x)}P_2O_5$ vitreous system. *J. Mater. Sci.,* 31, 1945–1967.

[25] Sreenivasu, D., Chandramouli, V. (200). Spectroscopic and transport properties of Cu^{2+} ion doped in (40-x)$Li_2O_{-x}LiF_{-60}Bi_2O_3$ glasses. *Bull. Mater. Sci.,* 23, 509–513.

[26] Dimitrov, V., Dimitriev, Y. (1990). Structure of glasses in PbO-V_2O_5 system. *J. Non-Cryst. Solids,* 122, 133−138.

[27] Dachille, F., Roy, R. (1959). A New High-pressure Form of B_2O_3 and Inferences on Cation Coordination from Infrared Spectroscopy. *J. American Ceramic Society.,* 42, 78−80.

[28] Iordanova, R., Dimitriev, Y., Dimitrov, V., Kassabov, S., Klissurski, D. (1996). Glass formation and structure in the $V_2O_5Bi_2O_3Fe_2O_3$ glasses. *J. Non-Cryst. Solids,* 204, 141–150.

[29] Montagne, L., Palavit, G., Mairesse, G. (1996). ^{31}P MAS NMR and FT IR analysis of (50-x/2) Na_2O. xBi_2O_3.(50-x/2) P_2O_5 glasses. *Phys. Chem. Glasses,* 37, 206−211.

[30] Moustafa, Y.M., El-Egili, K., Doweidar, H., Abbas, I. (2004). Phase equilibria in iron phosphate system. *Physica B,* 353, 82−91.

[31] Baia, L., Stefan, R., Kiefer, W., Simon, S. (2005). Structural characteristics of B_2O_3–Bi_2O_3 glasses with high transition metal oxide content. *J. Raman Spectrosc.,* 36, 262−266.

[32] Kamitsos, E.I., Chryssikos, G.D., Karakassides, M.A. (1987). Vibrational-spectra of magnesium-sodium-borate glasses. 1. Far-infrared investigation of the cation-site interactions. *J. Phys. Chem.,* 91, 1067−1073.

[33] Wang, M., Zhang, T.T., Song, Z.G. (2011). Eco-friendly Synthesis of 2-substituted-2,3-

dihydro-4(1H)-quinazolinones in water. *Chinese Chem. Lett.,* 22, 427−430.

[34] Safaei-Ghomi, J., Teymuri, R. (2019). A Three-component Process for the Synthesis of 2,3-dihydroquinazolin-4(1H)-one Derivatives Using Nanosized Nickel Aluminate Spinel Crystals as Highly Efficient Catalysts. *J. Chin. Chem. Soc.,* 66, 1490−1498.

[35] Rostami, A., Tavakoli, A. (2011). Sulfamic acid as a reusable and green catalyst for efficient and simple synthesis of 2-substituted-2,3-dihydroquinazolin-4(1H)-ones in water or methanol. *Chinese Chem. Lett.*, 22, 1317−1320.

[36] Benzekri, Z., Serrar, H., Boukhris, S., Souizi, A. (2017). $FeCl_3$/Egg Shell: An effective catalytic system for the synthesis of 2,3-dihydroquinazolin-4(1H)-ones at room temperature. *J. Turk Chem. Soc. Sect. A: Chem.,* 4, 775−786.

[37] Merroun, Y., Chehab, S., Ghailane, T., Boukhris, S., Ghailane, R., Habbadi, N., Hassikou, A., Lakhrissi, B., Souizi, A. (2018). An effective method to synthesize 2,3-dihydroquinazolin-4 (1H)-One using phosphate fertilizers (MAP, DAP and TSP) as green heterogeneous catalysts. *J. Turk. Chem. Soc. Sect A: Chem.,* 5, 303−316.

[38] Karhale, S., Survase, D., Bhat, R., Ubale, P., Helavi, V. (2017). A Practical and Green Protocol for the Synthesis of 2,3-Dihydroquinazolin-4(1H)-Ones Using Oxalic Acid as Organocatalyst. *Res. Chem. Intermed.,* 43, 3915−3924.

[39] Yassaghi, G., Davoodnia, A., Allameh, S., Zare-Bidaki, A., Tavakoli-Hoseini, N. (2012). Preparation, Characterization and First Application of Aerosil Silica Supported Acidic Ionic Liquid as a Reusable Heterogeneous Catalyst for the Synthesis of 2,3-Dihydroquinazolin-4(1H)-Ones. *B. Korean Chem. Soc.,* 33, 2724–2730.

[40] Yerram, P., Chowrasia, R., Seeka, S., Tangenda, S.J. (2013). Polyethylene Glycol (PEG-400) as a Medium for Novel and Efficient Synthesis of 2-Phenyl-2,3-Dihydroquinazolin-4(1H)-One Derivatives. *Eur. J. Chem.,* 4, 462–466.

[41] Sathe, B.P., Phatak, P.S., Kadam, A.Y., Gulmire, A.V., Narvade, P.R., Haval, K.P. (2018). An Efficient Synthesis of Substituted-2, 3-Dihydroquinazolin-4(1H)-Ones Using Fe_3O_4@SiO_2SO_3H Nano-Catalyst. *Int. Res. J. Sci. Eng.*, A5, 99−104.

[42] Zaghaghi, Z., Mirjalili, B.B.F., Monfared, A. (2019). Synthesis of 2,3-Dihydroquinazolin -4(1H)-Ones Promoted by Polystyrene Sulfonic Acid. *Org. Chem. Res.,* 5, 80−86.

[43] Katla, R., Chowrasia, R., da Silva, C., de Oliveira, A., dos Santos, B., Domingues, N. (2017). Recyclable $[Ce(L\text{-}Pro)_2]_2$ (Oxa) Used as Heterogeneous Catalyst: One-Pot Synthesis of 2,3-Dihydroquinazolin-4(1H)-Ones in Ethanol. *Synthesis*, 49, 5143−5148.